J. Fluid Mech. (1986), *vol.* 172, *pp.* 481–497
Printed in Great Britain

Gravity-driven flows in a turbulent fluid

By P. F. LINDEN AND J. E. SIMPSON

Department of Applied Mathematics & Theoretical Physics, University of Cambridge, Silver Street, Cambridge, CB3 9EW, UK

(Received 1 October 1985 and in revised form 4 June 1986)

The formation and destruction of a gravity current in a turbulent fluid is examined in laboratory experiments. The gravity current is produced by lock exchange and the fluid is kept turbulent by bubbling air from the base of the tank. When the lock is released the buoyancy forces associated with the reduced gravity g' between the fluid on the two sides of the lock drives a counterflow, with the dense fluid slumping underneath the less-dense fluid, and a gravity current is formed. The current has a sharp density front at its leading edge, and a stable density stratification is established behind the front. The turbulence, characterized by a longitudinal turbulent diffusion coefficient K, tends to mix this stable stratification. Once the fluid is vertically mixed the gravity current front is destroyed, and the density varies smoothly with horizontal distance over a zone whose length increases with time owing to the continuing longitudinal turbulent diffusion and buoyancy driving. It is found that the gravity current propagates over a distance L_1 before it is destroyed, where $L_1/H \approx 0.08(g'H)^{\frac{1}{2}}H/K$, and H is the fluid depth. At this point turbulent dissipation balances the buoyancy driving and frontogenesis is inhibited. The turbulent dispersion coefficient is found to increase with the buoyancy driving with $K \propto Ri^{\frac{1}{2}}$, where $Ri = g'H/q^2$ and q is the r.m.s. turbulence velocity fluctuations. It is also shown that when the turbulence level is reduced nonlinearities in the horizontal density gradient can sharpen up to form a front. The implications of these frontogenetical processes to the sea-breeze front and fronts in shallow seas is discussed.

1. Introduction

Frontogenesis, the sharpening up of horizontal gradients to form a front, occurs in a number of natural flows. In estuarine regions horizontal gradients of salinity between the fresh river water and the sea are observed to sharpen up to form one, or sometimes multiple, fronts. These can often be observed as lines of foam or debris that accumulate as a result of convergence at the front. In the atmosphere, sea-breeze fronts form, usually in the latter part of the afternoon, and travel large distances inland.

The formation of the sea-breeze front, in which there are abrupt changes in the temperature and humidity between the sea air and the air further inland, provides a clear example of frontogenesis. During the early part of a day with no strong synoptic winds the sea air progressively warms as it moves inland and there is not a clearly definable front. It is only later in the day that the front forms and it may then travel several hundred km from the coast. There has been considerable debate about the mechanisms that cause the front to form: see, for example, the recent review by Simpson (1982). It has been suggested that it is necessary that the synoptic

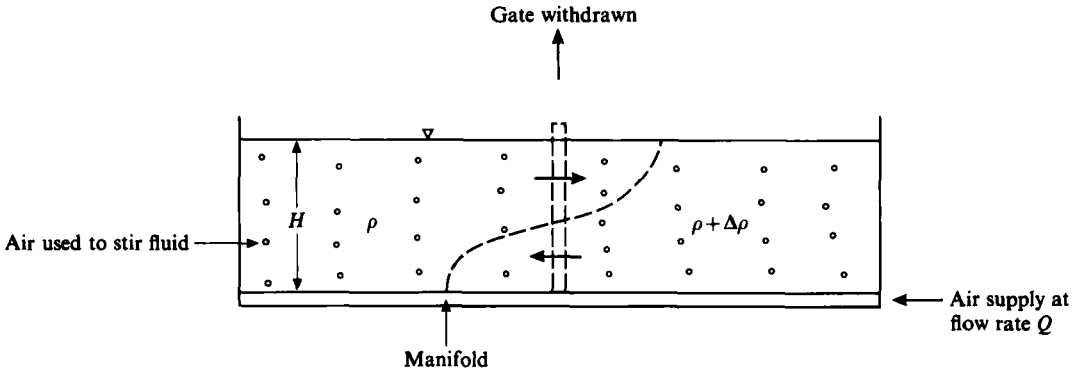

FIGURE 1. A sketch of the experimental apparatus.

winds must oppose the sea breeze before a front will form. An alternative suggestion (Simpson, Mansfield & Milford 1977) is that the tightening up of the front results from an increase in the horizontal temperature differences later in the day. While these mechanisms are undoubtedly important under some circumstances, we shall show that they are not essential for frontogenesis. Indeed, sea-breeze fronts have been observed on days when the synoptic winds are onshore (Pedgley 1958; Clarke 1973). In these cases the fronts only developed at distances greater than 20 km inland. One process which has received relatively little attention is the effect of background turbulence on the formation and dissipation of a front. In the sea breeze the turbulence results from convective motions in the atmospheric boundary layer. Wallington (1961) presented observations of the sea breeze in southern England which suggest that the abruptness with which the sea breeze sets in is related to the depth of the atmospheric surface layer. The onset was observed to be sharper on a day with deeper convection compared with a more gradual onset when the convective depth is limited, for example by anticyclonic subsidence, to a relatively shallow layer. In estuaries and coastal regions the turbulence is generated primarily by tidal flows and also by the wind. The possible effects of turbulent mixing can be seen by considering the situation sketched on figure 1, where two regions of fluid with different, but uniform, densities are separated by a vertical barrier. When the barrier is removed the well-known exchange flow develops with gravity currents travelling in opposite directions away from the barrier. One such current is shown on figure 2. The features of this classical flow that are important to the present discussion are the sharp fronts which form at the leading edges of the gravity currents. These are sustained by a convergent flow towards the leading edge which, in turn, is balanced by mixing at the head (Britter & Simpson 1978). In addition the region between the two diverging heads is stably stratified and very little mixing takes place between the two streams in this region. One consequence of this lack of exchange of mass and momentum is that the horizontal density flux across a vertical plane such as at the position of the now absent barrier is large.

Now suppose that instead of allowing the gravity currents to move in quiescent surroundings the fluid is stirred in some way so as to maintain a constant level of turbulence. When the barrier is removed, the dense fluid will slump underneath the lighter fluid as in the initial phases of the gravity current formation. But, if the turbulence is vigorous enough the resulting vertical stratification will be rapidly destroyed and a region centred on the barrier position with horizontal but no mean

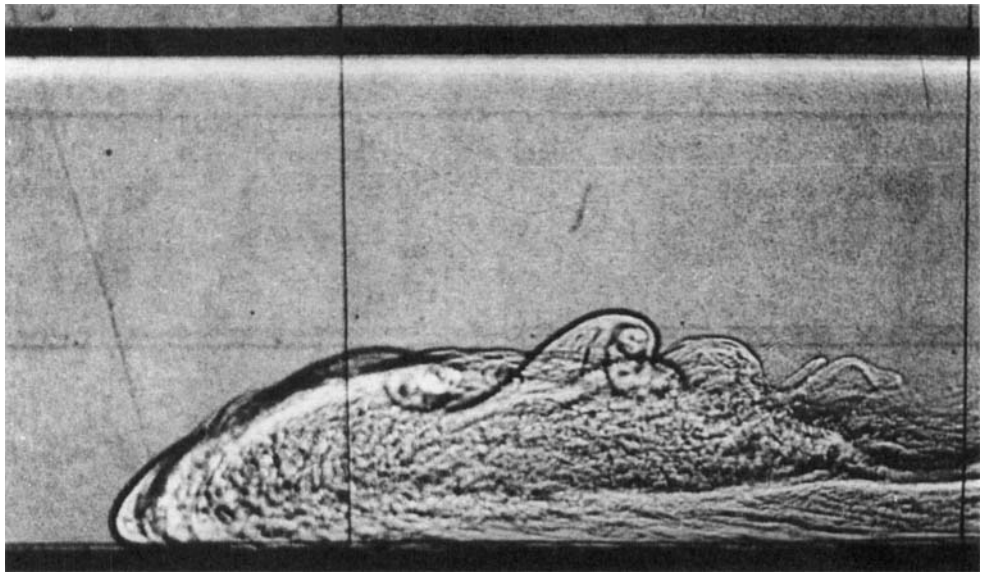

FIGURE 2. A gravity current produced by lock exchange in an undisturbed fluid with $g' = 9.8$ cm s^{-2} and $H = 8$ cm. Note the sharp 'front' at the leading edge. The direction of propagation is from right to left.

vertical density gradients will be produced. This region will expand with time as a result of the combined effects of turbulent stirring and buoyancy-driven circulation. There is, in this case, only a gradual transition between the two extreme densities and frontogenesis is inhibited by the background turbulence. We suggest, therefore, that the level of background turbulence affects the tendency of horizontal density gradients to sharpen up to form a front. In the case of the sea breeze the level of convective turbulence decreases in the late afternoon and it is at this time that the sea breeze front forms on days with light synoptic winds. Observations of a front in Liverpool Bay made by Czitrom Baus (1982) show that the strength of the vertical stratification varies with the magnitude of the tidal flow.

The aim of this paper is to determine the conditions under which turbulent mixing can inhibit frontogenesis, and to examine the properties of the flow resulting from the combined effects of a horizontal density gradient and background turbulence. Laboratory experiments of the dam-break flow described above are used to investigate these questions. Particular attention is paid to the unsteady aspects of the flow, in its early stages when there is a transition from a gravity current to a vertically mixed state and also the response of this mixed state to reductions in the level of turbulent stirring.

The previous work that is most closely related to the present investigation is that of Harleman & Ippen (1960) who examined the steady salinity distribution in a turbulent stream. Salt solution was introduced into the downstream end of a current of fresh water in a laboratory flume, and turbulence was maintained throughout the depth of the water by the vertical oscillation of a stack of horizontal grids. From measurements of the salinity distribution upstream of the source an effective diffusion coefficient was determined. They found that for passive inputs the upstream diffusion increased with increased stirring, but that it decreased with increased stirring for dense inputs, a result which is perhaps counter-intuitive. As expected the

diffusion coefficient was found to increase with increasing density differences. Harleman & Ippen's experiments only included cases where there was total vertical mixing and the question of frontogenesis was not addressed.

The other study closely related to this work is that of Thomas & Simpson (1985). They investigated the effect of turbulence generated by an oscillating grid on a gravity current. One essential difference between that study and the present one is that the grid, which was in a horizontal plane and executed vertical vibrations of small amplitude compared to the fluid depth, produced turbulence which decayed with distance from the grid. In that sense it provides a more realistic model of shear generation of turbulence in a naturally occurring flow than the bubbles do. On the other hand, that spatial decay of the turbulence has some features which the present work wished to avoid. Also it is more difficult to achieve the low values of the Richardson number using an oscillating grid.

The plan of the paper is as follows. In §2 the experiments are described and the rationale for the particular configuration we used is given. The characterization of the turbulence in terms of an effective longitudinal diffusion coefficient for a passive scalar is described in §3. A description of the gravity-current phase and the effects of the stirring is given in §4 and in §5 the results from the vertically mixed phases are presented. In a number of experiments the turbulence level was decreased during the vertically mixed phase. The buoyancy-driven circulation increased, the fluid became stably stratified and frontogenesis was observed. These experiments are discussed in §6, and in §7 we examine the implications of the results for the formation and dissipation of small-scale fronts in the atmosphere and ocean.

2. The experiments

The experiments were carried out in a rectangular Perspex tank 10 cm wide, 180 cm long and with a working depth of 15 cm sketched on figure 1. It was fitted with a removable vertical partition placed across the middle of the tank. Salt solution was placed on one side of the barrier and fresh water on the other, and the pressure on the two sides was equalized. The flow was visualized using a shadowgraph and by adding a small amount of dye to the fluid on one side of the barrier. A visual record of the flow was made using still photography and with a video camera.

The fluid on both sides of the barrier was stirred by bubbling air from a regular array of holes in a manifold in the base of the tank. The holes were of 0.1 cm diameter and spaced at 2.5 cm intervals along the centrelines of 1.5 cm square tubes. These tubes were connected to a compressed-air supply and the flow rate monitored by a flow meter. Provided the air flow rate was not too large the bubbles rose almost vertically and a uniform level of turbulence was achieved throughout the tank. At high flow rates the bubbles collected into convective cells, and this limited the vigour of the turbulence that could be produced. Bubbles were used to produce the turbulence since we wanted the turbulent intensity to be approximately uniform throughout the depth of the fluid. In situations where the turbulence decays with depth, such as when it is produced by an oscillating grid, there is a tendency for vertical density gradients to be sharpened as has been noted by Thomas & Simpson (1985).

Another reason for using bubbles to generate the turbulence, rather than grids as Harleman & Ippen had done, was because it was felt that a stack of grids would produce a high resistance to the flow. Bubbles are simple to produce and there are no temporal oscillations of the turbulence intensity associated with the vibration of

grids. Both methods share the disadvantage that the forcing continues regardless of the strength of any vertical stratification that may develop. Even so, there is some feedback between the turbulence and the stratification as the turbulence is generated in the bubble wakes (or in the wakes of the grid bars) and the ability of this turbulence to mix fluid decreases in stable conditions (Linden 1980).

In addition to visual observations of the flow, measurements of the salinity distribution were made using a suction conductivity probe mounted on a trolley which ran on rails above the tank. A traverse mechanism was mounted on the trolley which enabled the probe to be moved in any direction. The probe was calibrated before and after each experiment but no significant drift was recorded. The position of the probe was monitored using potentiometers mounted on the traverse, and the output of both the probe and the potentiometers were recorded on a BBC microcomputer. In most cases the probe was positioned at mid-depth and was driven back and forth along the length of the tank. In a few runs the vertical homogeneity of the fluid was measured. Sampling rates up to 10 Hz were used giving a spatial resolution along the tank of 0.25 cm.

The strength of the buoyancy driving is characterized by $g' = g\Delta\rho/\rho$, where $\Delta\rho/\rho$ is the fractional density difference between the salt and fresh water before the barrier is removed and g is the acceleration due to gravity. In stationary surroundings of depth H the two gravity-current fronts move in opposite directions at constant speeds. The dense current travels with velocity $U = 0.46(g'H)^{\frac{1}{2}}$, provided the Reynolds number $Re = UH/\nu > 500$ (Simpson & Britter 1979). In these experiments g' varied between 5 and 50 cm s^{-2} and the fluid depth H was in the range 6–12 cm, giving values of Re from 400 to 1500. At the lower end of the range viscous effects may start to be significant.

3. Characterization of the turbulence

In order to characterize the turbulence produced by the rising bubbles a number of experiments were carried out to determine the effective diffusivity of the turbulence when buoyancy effects are absent. This was done by placing a salt solution on one side of the barrier and a sugar solution on the other. The densities were carefully matched (to 1 part in 10^4) before removing the barrier. Since sugar concentration has only a very weak effect on the conductivity, the longitudinal turbulent diffusion of the salt is readily determined using the conductivity probe. (Low concentrations of sugar and salt were used to avoid any double-diffusive effects.)

Plots of salt concentration $S(x,t)$ against distance x along the tank at a number of different times t for a passive tracer ($g' = 0$) and a fixed value of the air flow rate Q are shown on figure 3. These profiles show the smearing of the initial step in salinity concentration by the turbulence and the subsequent longitudinal transport of the salt. Assuming that this turbulent transport can be represented as a Fickian process with a constant effective difussion coefficient K, then $S(x,t)$ satisfies

$$S_t = KS_{xx}. \tag{3.1}$$

Initially the salinity is given by

$$S(x,0) = \begin{cases} S_0, & 0 < x \leqslant \frac{1}{2}L, \\ 0, & -\frac{1}{2}L \leqslant x < 0, \end{cases} \tag{3.2}$$

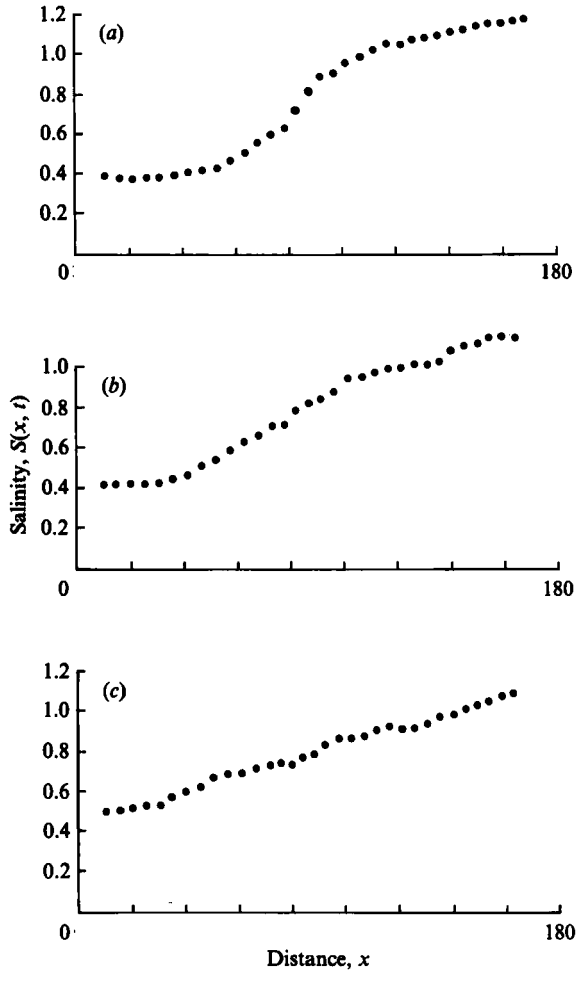

FIGURE 3. The salinity $S(x,t)‰$ plotted against distance x cm along the tank for 3 different times during a run: (*a*) $t = 2$ min; (*b*) 4 min; (*c*) 20 min. The position of the gate was at $x = 90$ cm. The spreading of the salinity step and the subsequent longitudinal transport is produced by the bubble-induced turbulence since buoyancy forces are absent ($g' = 0$). The other parameters are $H = 12$ cm and the air flow rate per unit area $Q/A = 0.09$ cm s^{-1}.

and the no-flux conditions implied by the solid ends of the tank are

$$S_x(\pm\tfrac{1}{2}L, t) = 0. \tag{3.3}$$

The subsequent salinity distribution $S(x,t)$ satisfying (3.1)–(3.3) is

$$S(x,t) = S_0 + 2S_0 \sum_{n=0}^{\infty} (2n+1)^{-1} \exp\left\{-\left[\frac{(2n+1)\pi}{L}\right]^2 3Kt\right\} \sin(2n+1)\frac{\pi x}{L}. \tag{3.4}$$

At large times $t \gg L^2/(8\pi^2 K)(\approx 100$ s) an adequate approximation to (3.4) is obtained from the first term, in which case

$$\frac{\pi^2 Kt}{L^2} = -\ln\left(1 - \frac{2S(-\tfrac{1}{2}L, t)}{S_0}\right). \tag{3.5}$$

An example of one of the passive-scalar experiments is shown on figure 4, where the

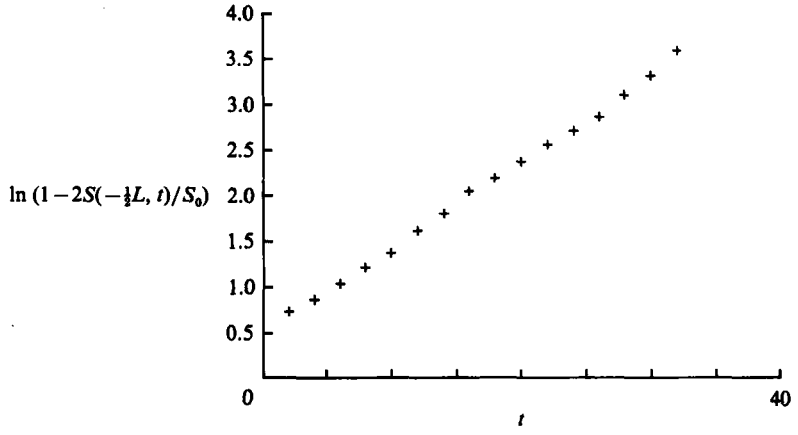

FIGURE 4. Analysis of the passive-scalar experiment shown on figure 3, where $-\ln(1-2S(-\frac{1}{2}L, t)/S_0)$ is plotted against t. The fact that the data lie on a straight line shows that the longitudinal transport process is described by a constant eddy diffusivity.

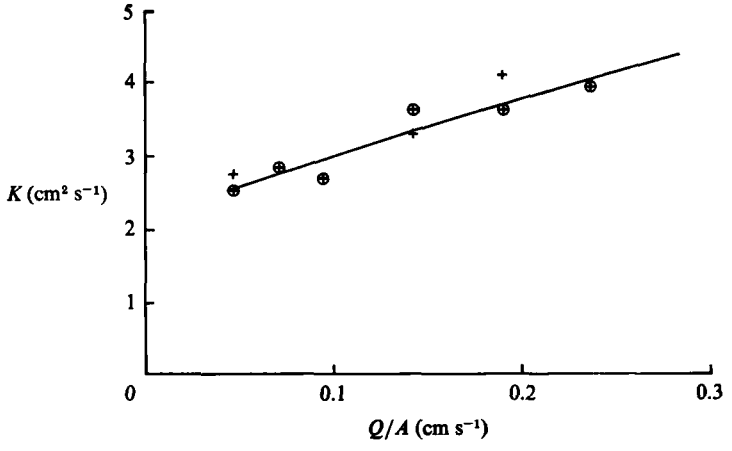

FIGURE 5. The diffusivity K cm^2 s^{-1} for the passive runs plotted against Q/A cm s^{-1} the air flow rate per unit area. +, $H = 12$ cm; ⊕, $H = 6$ cm. The curve is a quadratic least-squares fit to the data.

right-hand side of (3.5) is plotted as a function of time t. The experimental points are accurately described by a straight line, indicating that the assumption of Fickian diffusion seems to be appropriate. The diffusivity K is determined from the slopes of these lines and the results are shown on figure 5, where K is plotted against Q, the flux of air.

The turbulence is mainly produced by the bubble wakes, and so has velocity scale comparable with the bubble rise velocity q and a lengthscale l comparable with the radius of the bubbles a. A volume flux Q of air is forced out of N holes per unit area in the base of the tank. If the spacing between the bubbles originating from a particular hole is $\approx 2a$, a result which is consistent with the surface-tension instability producing the bubbles and with our observations, then the number of bubbles produced per unit time is $q/4a$. Hence the flux of air from a single hole is

$$\frac{Q}{N} = \frac{\frac{1}{3}\pi a^3 q}{a}. \tag{3.6}$$

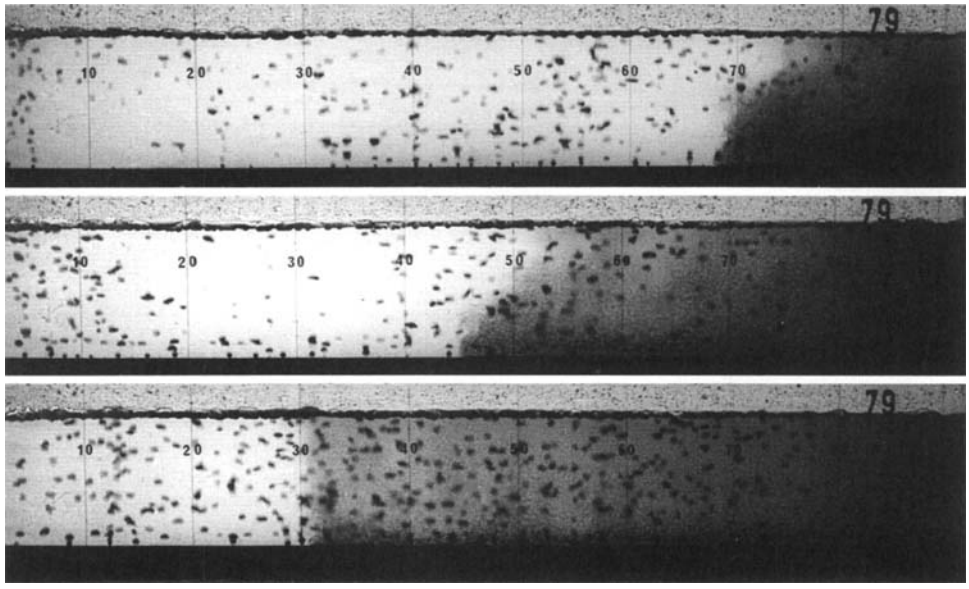

FIGURE 6. The evolution of a gravity current in the presence of ambient turbulence. The initial buoyancy difference $g' = 20.0$ cm s^{-2}, $H = 12$ cm and $Q/A = 0.09$ cm s^{-1}. The photographs were taken at (*a*) 4.2 s; (*b*) 8.9 s; (*c*) 12.7 s after the removal of the gate. The thin stable layer near the bottom in (*c*) disappears at a later time and no persistent vertical stratification is visible.

With a bubble rise velocity $q = \frac{2}{3}(ga)^{\frac{1}{2}}$, we get

$$q = 0.7\left(\frac{g^2 A}{N}\right)^{\frac{1}{5}}. \tag{3.7}$$

The diffusivity $K \approx qa$, and so (3.7) predicts no dependence of K on the fluid depth H and a weak dependence on Q as is observed in figure 5. A least-squares fit to the data over the range $0.03 < Q/A < 0.3$ cm s^{-1}, where A is the area of the tank base, is shown on figure 5 and this curve was used to estimate K for a given air flow rate Q. For buoyant flows ($g' \neq 0$) we use the Richardson number $Ri = g'H/q^2$ as a measure of the density driving. The value of q is not measured directly but is given by K/a, while K is taken from the passive data on figure 5. Then $Ri \approx 4U^2/q^2$ where U is the speed of the undisturbed current.

4. The gravity-current phase

When the barrier is removed a circulation is driven by the buoyancy forces associated with the density differences originally set up between the sides of the barrier, with the denser fluid tending to run underneath the lighter fluid. This initial acceleration is produced by the horizontal pressure gradient, which in the idealized case of a barrier of zero thickness takes the form of a delta function at the interface between the two fluids. Even in the experiment this pressure gradient is very large and the flow is rapidly accelerated. The gravity-current phase is shown on figure 6 (*a*). As the gravity current moves along the tank the turbulence mixes it with its surroundings, thereby reducing the density difference between the current and the environment. This process can be seen on figure 6 (*b*, *c*) where the gradual incorporation of the dyed fluid in the dense current into the fluid above is shown. Eventu-

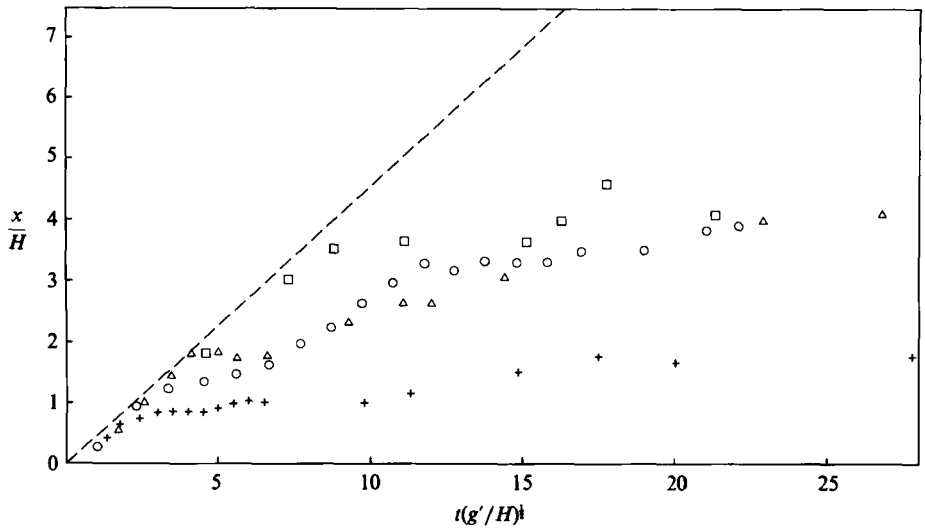

FIGURE 7. The position x of the front, non-dimensionalized by the depth H, plotted against the dimensionless time $t(g'/H)^{\frac{1}{2}}$. The position of the leading edge of a gravity current travelling down a channel in calm surroundings is shown by the broken line. For the data shown the turbulence intensity is constant at $q = 5.7$ cm s^{-1} and $H = 12$ cm. +, $g' = 3.1$ cm s^{-2}; △, 6.7 cm s^{-2}; ○, 12.6 cm s^{-2}; □, 15.6 cm s^{-2}.

ally, the fluid becomes vertically mixed and the density gradients are horizontal in a transition zone centred on the initial interface position. Provided that the vertical mixing is complete before dense fluid reaches the end of the tank, the situation has then reverted to the original state except that the horizontal pressure gradient is much reduced. The density difference between the fluids on either side of the transition zone is the same as at the start, but the width of the zone is much greater than the initial vertical interface. Thus it is the magnitude of the horizontal pressure gradient, and not simply the overall density difference, that determines the buoyancy driving. In a classical gravity current as shown in figure 2 the density is almost uniform up to the front and so the very large horizontal pressure gradient is maintained throughout its motion.

The transition zone continues to increase in length after the vertical mixing is complete owing to the combined effect of turbulent stirring and a relatively weak buoyancy-driven circulation. In the early stages of this growth the dye was observed to maintain a relatively well-defined vertical front the approach to which is shown on figure 6(*c*). The position x/H, where x is measured from the barrier, of this dye front, which coincides with the leading edge of the gravity current before it is mixed, is plotted on figure 7 against the dimensionless time $t(g'H)^{\frac{1}{2}}$ for four runs. The result for the advance of a gravity current into still surroundings is shown by the broken line and it can be seen that the data conform to this line in the initial stages after the barrier is removed. At later times, as the turbulence mixes the current with its surroundings, the front velocity is reduced. The departure from the undisturbed current speed occurs further downstream for higher values of g' when buoyancy forces are stronger. By examining plots such as these for each experiment to determine the point of departure from the undisturbed gravity-current line it is possible to ascertain the point of transition L_1 from the gravity-current phase.

Suppose that the effect of the turbulence can be described in terms of an eddy

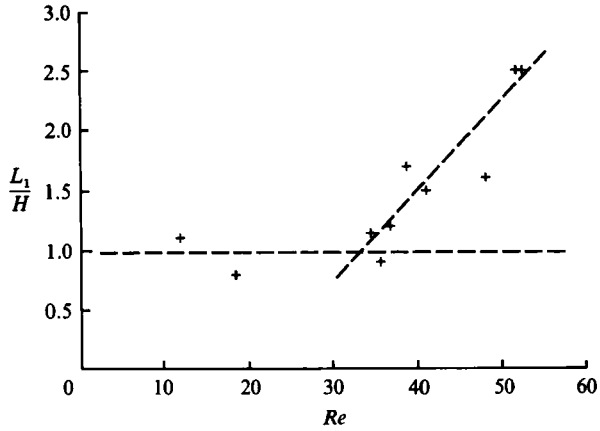

FIGURE 8. The dimensionless limit L_1/H of the gravity-current phase plotted against the turbulent Reynolds number $Re = (g'H)^{\frac{1}{2}}H/K$. The broken lines are a suggested interpretation of the data, as described in the text.

viscosity K_m. As a first approximation we suppose that the turbulence is unaffected by the stratification and that Reynolds' analogy applies so that K gives an adequate estimate for K_m. In practice this turns out to be a reasonable estimate since once the gravity-current phase is complete the vertical stratification is very weak. At the end of the gravity-current phase then, the flow has a mean horizontal circulation $U(z)$ flowing in opposite directions in the upper and lower halves of the tank. This counterflow is driven by a horizontal pressure gradient $g'H/L_1$, where L_1 is the transition point determined from figure 7, and is described by

$$KU_{zz} = -g'H/L_1. \tag{4.1}$$

Solving (4.1) in the lower half of the channel with the boundary conditions $U(0) = U(\frac{1}{2}H) = 0$ gives the mean horizontal velocity $\bar{U}$ as

$$\bar{U} = \frac{g'H^3}{48KL_1}. \tag{4.2}$$

If we postulate that the gravity-current phase ends when the horizontal pressure gradient is reduced to the extent that $\bar{U}$ becomes comparable with the undisturbed gravity current speed $0.5(g'H)^{\frac{1}{2}}$, then we estimate L_1 to be

$$\frac{L_1}{H} = \frac{(g'H)^{\frac{1}{2}}H}{24K}. \tag{4.3}$$

The results of the experiments are shown on figure 8 where the transition point L_1/H is plotted against the turbulent Reynolds number $Re = (g'H)^{\frac{1}{2}}H/K$. For small values of Re the transition takes place very rapidly, although it appears that the interface slumps through a distance comparable with the fluid depth no matter how hard it is stirred. At larger values of Re, L_1/H increases approximately linearly with increasing Re. These trends are indicated by the broken lines shown on figure 8, which are drawn through the data by eye. The experimental results shown on figure 8 correlate well with this parameter, although the constant of proportionality 0.08 is larger than predicted by (4.3).

An alternative derivation of (4.3) suggested to us by Dr R. Kimura is to consider the time T taken to mix the gravity current through the depth H by a diffusion

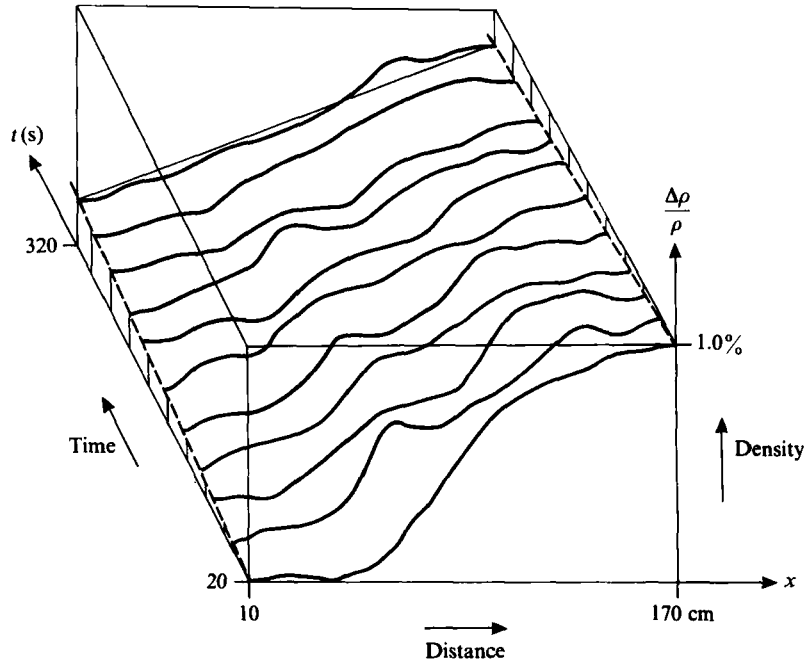

FIGURE 9. The evolution of the horizontal density distribution for the case $Q/A = 0.09$ cm s^{-1}, $g' = 9.8$ cm s^{-2} and $H = 12$ cm. The probe does not sample the extreme 10 cm at either end of the tank, owing to the design of the traversing mechanism.

processes with diffusivity K, i.e. $T \approx H^2/K$. In this time the current will have travelled with speed $U = 0.5(g'H)^{\frac{1}{2}}$ a distance $L_1 \approx 0.5(g'H)^{\frac{1}{2}}H^2/K$, as before.

5. The vertically mixed phase

Once the fluid is vertically mixed the transition zone between the two extreme densities continues to increase in length as a result of turbulent mixing and a buoyancy-driven circulation, until it eventually occupies the full length of the tank, after which salt continues to be transported down the gradient until, eventually, the concentration is uniform throughout the fluid. An example of this process is shown on figure 9 which displays a set of horizontal density profiles taken at various times during a single experiment. In the earliest profiles the fluid still retains some vertical stratification and the transition zone is confined near the centre of the tank. But within a relatively short time the zone extends over the whole tank, the fluid is vertically mixed and the densities at the ends of the tank begin to change.

If we assume that the horizontal transport of salt can still be described as a Fickian process with a constant diffusion coefficient when buoyancy effects are significant, then we can estimate the effective diffusivity K in the manner described in §3 for the passive tracer. In this case $K = K(Ri)$. Figure 10 shows a number of experiments plotted in the form of (3.5). In this case the data do not follow a straight line over the whole run since the density difference decreases appreciably over the duration of an experiment. But sections of the data can be approximated by straight lines and this was done and the diffusivities calculated as for the passive scalar.

The diffusitives $K(Ri)/K(0)$, non-dimensionalized by the values for the passive case appropriate for the particular air flow rate and depth, are shown on figure 11. The

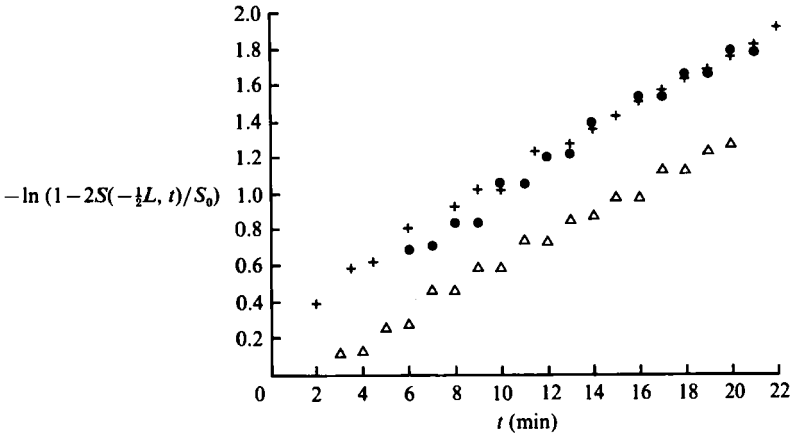

FIGURE 10. Plots of $-\ln(1-2S(-\frac{1}{2}L,t)/S_0)$ against time t for three runs with significant buoyancy-driven circulation. $H = 6$ cm, $Q/A = 1.2$ cm s^{-1} and the *initial* values of g' are: +, 18.2 cm s^{-2}; ●, 17.0 cm s^{-2}; and △, 35.9 cm s^{-2}.

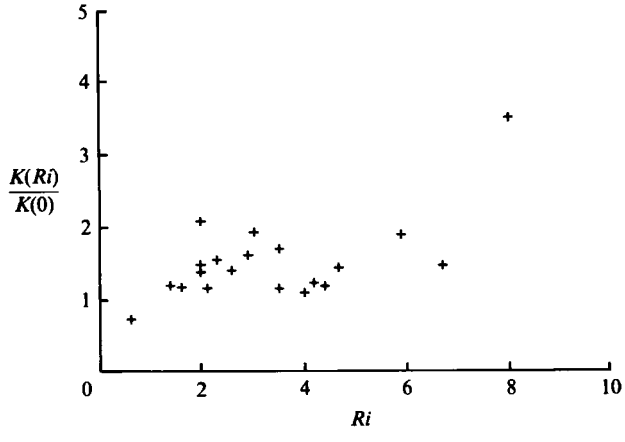

FIGURE 11. The 'diffusivity' $K(Ri)$, non-dimensionalized by the value $K(0)$ corresponding to the air flow rate for the given experiment, plotted against $Ri = g'H/q^2$. An estimate of the experimental uncertainty is provided by the scatter in the data.

data exhibit a considerable degree of scatter but show that $K(Ri)$ increases with increasing Ri, reflecting the enhanced flux of density with increasing density difference. A least-squares fit of this data suggest that

$$\frac{K(Ri)-K(0)}{K(0)} = 0.22\,Ri^{0.55}. \tag{5.1}$$

It is instructive to compare the values of $K(Ri)$ with those obtained from the undisturbed gravity current which corresponds to $Ri = \infty$. The horizontal buoyancy flux produced by a gravity current is $0.23(g'H)^{\frac{3}{2}}$. An estimate of the 'diffusivity' $K(\infty)$ of the gravity current is then obtained using the horizontal buoyancy gradient g'/L_1 as given by (4.3). This gives

$$\frac{K(\infty)}{K(Ri)} = \frac{0.01g'H^3}{K(0)\,K(Ri)}. \tag{5.2}$$

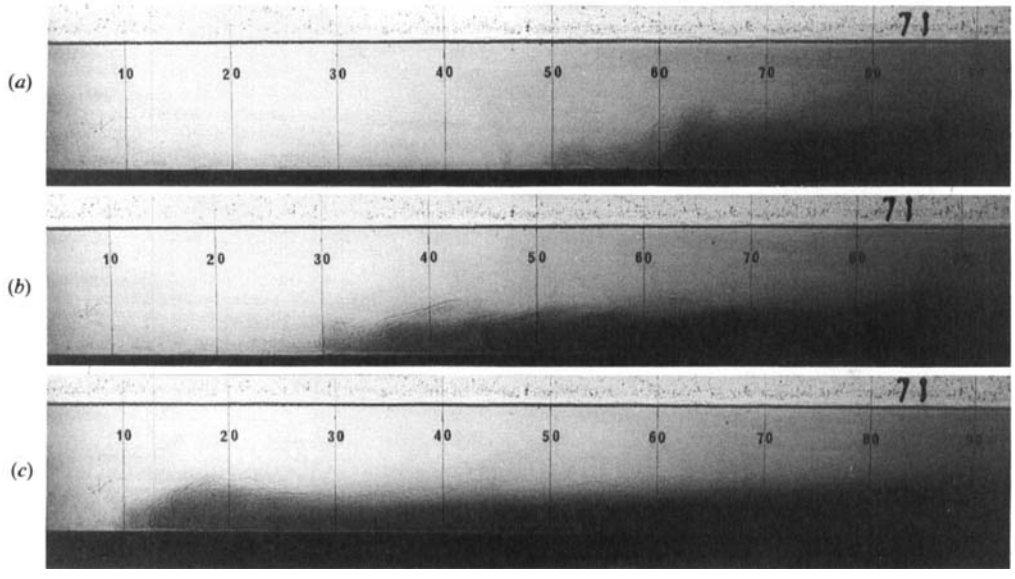

FIGURE 12. Frontogenesis, the formation of a gravity current after the turbulence ceases. In this example the fluid was vertically mixed and the buoyancy difference between the ends of the tank when the bubbles were turned off was $g' = 5$ cm s^{-2}, the depth $H = 12$ cm. The photographs were taken at (*a*) 8.9 s. (*b*) 10.8 s and (*c*) 17.4 s after the bubbling stopped.

Typical values of the parameters from the experiments, $g' = 10$ cm s^{-2}, $H = 12$ cm and $K(0) = K(Ri) = 4$ cm^2 s^{-1}, show that $K(\infty)/K(Ri) \approx 10$. Thus the gravity current is much more effective at transporting salt horizontally and the addition of turbulence *decreases* that flux. A similar reduction in flux during the gravity-current phase when there is significant vertical stratification can also be inferred from the decrease in the speed of the current shown on figure 7.

6. Frontogenesis

In a number of the experiments the turbulence was turned off while there was still an appreciable horizontal density gradient. Under these circumstances frontogenesis and the formation of a gravity current was observed. An example of this process is shown on figure 12, which shows the formation and propagation of the gravity current in the left-hand half of the tank. A current consisting of less-dense fluid and propagating to the right was also observed in the right-hand half of the tank. In this instance dye was introduced near the centre of the tank (at $x = 90$ cm) when the turbulence was turned off. Immediately afterwards an accelerating counterflow began to develop and a vertical stratification was established. This counterflow continued to accelerate and eventually the structure of a gravity-current head was observed on the shadowgraph with sharp horizontal density gradients at the front. This current then propagated with relatively little further increase in velocity until it reached the endwall of the tank.

Measurements made with the conductivity probe placed near the endwall $x = -\frac{1}{2}L$ showed that the fluid immediately behind the front had originated at the far end ($x = \frac{1}{2}L$) of the tank. This fluid had travelled the full length of the tank with very little mixing, as is characteristic of gravity-current flows. Observations with dye

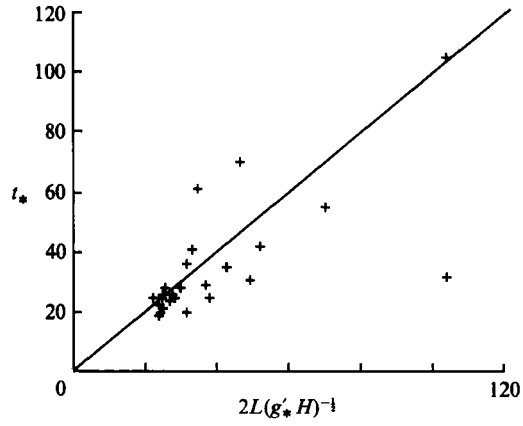

FIGURE 13. The time t_* of arrival of the leading edge of the dense current at the endwall $x = -\frac{1}{2}L$ plotted against the timescale $2L(g'_*H)^{-\frac{1}{2}}$. The time is measured from the instant when the bubbles are turned off, and g'_* is the buoyancy difference between the fluid at the ends of the tank at that time. The straight line is a graph of (6.3).

patches placed along the length of the tank supported these measurements and showed that the fluid from the dense end caught up to the front.

The time t_* of arrival of the front at the wall $x = -\frac{1}{2}L$ was measured from the time the bubbles were turned off. The results of these measurements are shown on figure 13, where t_* is plotted against the timescale $2L(g'_*H)^{-\frac{1}{2}}$, where $g'_* = g(\rho(-\frac{1}{2}L, t) - \rho(\frac{1}{2}L, t))/\rho(0, t)$ is the buoyancy difference between the fluid at the ends of the tank at the time the bubbling ceases.

Our studies (Linden & Simpson 1986) of the time evolution of a fluid with a *linear* variation of fluid density with horizontal position show that frontogenesis, the sharpening up of horizontal gradients, will only occur when the density gradients are initially nonlinear. In the case where there is simply a linear variation all points are equally likely to undergo frontogenesis and there is no reason to prefer one horizontal position to another. In the present experiments the regions near the two endwalls of the tank have the greatest nonlinearity in the density profile. The no-flux boundary condition (3.3) implies that the horizontal density gradient decreases towards zero at the ends of the tank. Some evidence of this diminution of the horizontal density gradient is seen in the profiles shown on figure 9. Consequently, the endwalls produce the nonlinearity required to initiate frontogenesis.

When the turbulence has decayed the dissipative processes associated with the vertical mixing of horizontal momentum becomes small and the horizontal pressure gradient accelerates the flow. The term KU_{zz} in (4.1) becomes negligible and the counterflow is described by

$$\tfrac{1}{2}(U^2)_z = g'_*. \tag{6.1}$$

Then, integrating (6.1) we find

$$U \approx 0.5(g'_*H)^{\frac{1}{2}}. \tag{6.2}$$

This speed is the usual gravity-current velocity in undisturbed surroundings where g'_* is the buoyancy difference between the ends of the tank. Assuming that the front travels at a constant speed given by (6.2), the time taken to traverse the tank of length L is

$$t_* = \frac{2L}{(g'_*H)^{\frac{1}{2}}}. \tag{6.3}$$

This result is shown on figure 13 and we see that it is in quite good agreement with the data.

7. Discussion

In this paper we have described some laboratory experiments on the dynamics of density-driven flows in the presence of background turbulence. We have shown that a gravity current produced by a lock exchange can be destroyed by externally imposed turbulence and have determined the level of turbulence required for a given amount of buoyancy driving.

The experiments clearly demonstrate that it is not the overall horizontal density *difference* that determines the strength of the buoyancy forces, but the magnitude of the horizontal density *gradient*. In a lock exchange this density gradient is very large initially, and in the absence of background turbulence the gravity-current flow maintains this large gradient at the front. Fluid is brought from the rear of the current with virtually no mixing with its environment since it is shielded from the surrounding fluid by stable density interface (Britter & Simpson 1978). Nearly all the mixing that occurs takes place at the head *after* the fluid has circulated past the nose of the current (see figure 2). In this way the density gradient at the front is maintained and, in a channel of uniform width, the current travels at constant speed.

The presence of the stable vertical stratification behind the front of the current is crucial to these dynamics, and any aspect of the flow which tends to destroy this stratification will weaken the gravity-current flow. The bubbles, by lifting dense fluid in their wakes, produce increased mixing of both mass and momentum between the current and its environment. As the dense current travels through this turbulent flow the density of the fluid arriving at the front is continuously reduced due to this mixing and the horizontal pressure gradient at the front diminishes and the current slows down. At the same time the current experiences a far greater drag due to the vertical transport of horizontal momentum by the turbulence. The supply of dense fluid in the current is reduced and the turbulence erodes an ever weakening vertical density gradient until eventually the fluid becomes vertically mixed.

In the vertically mixed state continuing horizontal transport of density is produced by a combination of turbulent stirring and a buoyancy-driven circulation. The presence of the horizontal density gradient increases the horizontal transport and gives an enhanced longitudinal diffusion coefficient which increases as $Ri^{0.55}$. This result contrasts with that of Prych (1970) who suggests that the diffusion coefficient increases at the greater rate of Ri^2 for longitudinal mixing of buoyant material in open-channel flow.

As we mentioned in §1 the work most closely related to the present study are the experiments carried out by Harleman & Ippen (1960). They considered the vertically mixed phase and determined the enhancement of the longitudinal dispersion due to horizontal buoyancy forces. They found that $K(Ri)/K(0)$ increases as $Ri^{\frac{1}{2}}$ (their equation (33) written in the present notation) in agreement with the present results. They also determined the length L_f of the salinity intrusion in the presence of a flowing stream and find that the length L_f increases as $Ri^{\frac{1}{2}}$ (their equation (38) again in our notation). This length determines the magnitude of the horizontal pressure gradient sufficient to balance the turbulent dissipation, and so can be compared with L_1, the gravity-current transition length given by (4.3). In a flowing stream $K \approx qH$, where H is the depth, and so $L_1/K \approx Ri^{\frac{1}{2}}$ in agreement with Harleman & Ippen's result.

Much of the motivation for the present study came from the questions raised in §1 concerning the formation of the sea-breeze front and the response of fronts in shallow seas to stirring produced by tidal currents. These fronts typically have short enough time- or lengthscales for Coriolis forces to be unimportant in much of the local dynamic balance, and so are adequately modelled without including the effects of rotation. In the case of the sea breeze, convection in the atmospheric surface layer has a value of eddy diffusivity $K = ku_*H$ of approximately 10 $m^2\ s^{-1}$: here u_* is the friction velocity, $H \approx 500$ m the depth of the atmospheric surface layer and k von Kármáns constant. With $g' \approx 10^{-1} m\ s^{-2}$ (corresponding to a land–sea temperature difference of $3K$), according to (4.3) $L_1/H \approx 10$, i.e. $L_1 \approx 5$ km. This means that the atmospheric convection will vertically mix the density driven flow within 5 km of the coast and frontogenesis will be inhibited. This result is consistent with the observation (Koschmieder 1936) that most of the temperature and humidity contrast is confined to within a few km of the coast.

It is only in the latter part of the day when the strength of convection diminishes that a well-defined front forms. Simpson *et al.* (1977) documented the path of the sea breeze as it moved inland from the southern coast of England in June 1973. They observed that although an onshore sea breeze was detected at the coast from 10.00 GMT the advance was 'difficult to define' in the area of 20 to 25 km inland during the period 12.00 to 14.00 GMT. It was only considerably later, around 17.00 GMT, that a sharp front had formed.

Observations of a density front in Liverpool Bay have been made by Czitrom Baus (1982). This front is produced by river runoff and Czitrom Baus has shown that the strength of the front is related to the strength of the tidal flow. During periods of neap tides the vertical stratification is strong, and there is a sharp surface front. During spring tides the front is much weaker and the water is vertically mixed. Typical values associated with Liverpool Bay are $H = 50$ m, $g' = 10\ m\ s^{-2}$ and $K = 2\ m^2\ s^{-1}$. Then (4.3) implies that $L_1/H = 0.6$, and so strong tidal flows can destroy an organized gravity current flow within 30 m or so. The timescale τ for mixing the vertical stratification is $L_1/0.5(g'H)^{\frac{1}{2}}$, and using the experimental value for L_1, we see that $\tau \approx 0.2H^2/K$. Using parameters appropriate to Liverpool Bay gives $\tau \approx 250$ s. This time is short compared with a tidal cycle and so we might expect to observe the strengthening and weakening of the front during a tidal cycle.

Frontogenesis is observed in these experiments when the turbulence is turned off. The gravity-driven flow accelerates and nonlinearities in the horizontal density gradient associated with the endwalls of the tank sharpen up to form a front. A classical gravity-current flow is established with the front associated with the leading edge. An implication of the observations of the arrival times of the front at the endwall of the tank is that the establishment of the gravity current is a rapid process. This feature is also observed for the acceleration of the front in lock-exchange. The present experiments are not particularly well suited to examine the quantitative aspects of the onset of the gravity-driven flow since it is linked with the decay of the turbulence. A more detailed study will be reported elsewhere (Linden & Simpson 1986).

The use of bubbles to generate a turbulent flow has a number of advantages. It is a simple and easily controlled technique, capable of various modifications such as the production of spatially inhomogeneous turbulence levels. It is open to some criticism as a model of natural turbulence. First the bubbles themselves are impervious to stable density stratification, and will rise through any stable interface. Thus it is not possible to model a situation where the stratification is strong enough

to inhibit the turbulence altogether in some parts of the flow. However, there will be some feedback on the turbulence, as the experiments with a grid falling through a stratified fluid have shown (Linden 1980). Secondly, the lengthscale of the turbulence produced by the bubbles is related to the size of the bubbles themselves rather than, say, the depth of the fluid layer. Both of these shortcomings imply that the numerical results should be applied to natural flows with caution, particularly in the case of turbulence generated by shear flow where the intensity of the turbulence decreases with distance from the boundary.

We are grateful to the technical staff of the DAMTP laboratory, D. C. Cheesley, D. Lipman and J. Sharpe for constructing the apparatus and for their help with the experiments, and to Dr R. Kimura for a number of stimulating discussions about this work. This work was supported by a grant from the Natural Environment Research Council.

REFERENCES

Britter, R. E. & Simpson, J. E. 1978 Experiments on the dynamics of a gravity current head. *J. Fluid Mech.* **88**, 223–240.

Clarke, R. H. 1973 A numerical model of the sea-breeze. *1st Austr. Conf. Heat & Mass Transfer. Monash University, Melbourne*, pp. 41–48.

Czitrom Baus, S. P. R. 1982 Density stratification and an associated front in Liverpool Bay. PhD dissertation, Marine Science Laboratory, UCNW.

Harleman, D. R. F. & Ippen, A. T. 1960 The turbulent diffusion and convection of saline water in an idealised estuary. *Pub No.* 51 Intl. Assoc. Sci. Hydrol. Commission of Surface Waters, pp. 362–378.

Koschmieder, H. 1936 Danziger Seewind Studien I. *Danziger Met. Fosch.* **8**, 1–44.

Linden, P. F. 1980 Mixing across a density interface produced by grid turbulence. *J. Fluid Mech.* **100**, 691–703.

Linden, P. F. & Simpson, J. E. 1986 The formation of fronts in a fluid with smooth horizontal density gradients. In preparation.

Pedgley, D. E. 1958 The summer sea-breeze at Ismailia. *Met. Office. Met. Rep.* **3**, no. 19.

Prych, E. A. 1970 Effects of density differences on lateral mixing in open channel flow. *Keck Lab. Hydraul. Res. Calif. Inst. Tech. KH-R-21.*

Simpson, J. E. 1982 Gravity currents in the laboratory, atmosphere and ocean. *Ann. Rev. Fluid Mech.* **14**, 213–234.

Simpson, J. E. & Britter, R. E. 1979 The dynamics of the head of a gravity current advancing along a horizontal surface. *J. Fluid Mech.* **94**, 477–495.

Simpson, J. E., Mansfield, D. A. & Milford, J. R. 1977 Inland penetration of sea-breeze fronts. *Q. J. R. Met. Soc.* **103**, 47–76.

Thomas, N. H. & Simpson, J. E. 1985 Mixing of gravity currents in turbulent surroundings: Laboratory studies and modelling implications. In *Turbulence and Diffusion in Stable Environments* (ed. J. C. R. Hunt), pp. 61–95. Clarendon.

Wallington, C. E. 1961 *Meteorology for glider pilots.* John Murray.